# The Origin of the Positive Effect of Cadmium Acetate on the Action of Supported Palladium Catalysts

**Steffi Adam, Andrea Bauer, Olaf Timpe, Ute Wild, Gerhard Mestl, Wolfgang Bensch, and Robert Schlögl***

**Abstract:** The complex chemistry of $Pd(OAc)_2$ and $Cd(OAc)_2$ in the solid state and in acetic acid solution has been studied. Triclinic crystals, space group $P\bar{1}$, of a new complex $[CdPd(CH_3COO)_4 \cdot CH_3COOH]_2$ were isolated from the solution. Palladium is square-planar coordinated by acetate ligands, with metal–oxygen bond lengths of approximately 200 pm, and has cadmium at one of its free axial coordination sites at a distance of 280 pm. Cadmium is coordinated by acetate ligands in a trigonal-prismatic geometry capped by palladium. UV/Vis spectroscopy confirmed the existence of the complex in solution as well as in the solid state. The thermal decomposition was characterised in detail by thermogravimetry coupled with mass spectrometric detection of the decomposition products and X-ray photoelectron spectroscopy (XPS). XPS revealed the presence of elemental Pd during thermal decomposition at 423 K. Thermal decomposition of the compound finally led to partially oxidised Pd and CdO. The application of $[CdPd(CH_3COO)_4 \cdot CH_3COOH]_2$ as a precursor in the synthesis of supported Pd catalysts influenced their catalytic activity positively in a test reaction (the total oxidation of ethylene), in comparison with catalysts prepared from binary palladium acetate. Transmission electron microscopy of the used catalysts revealed a significant improvement in Pd dispersion in the catalyst prepared from the complex, compared with the material prepared from Pd acetate.

**Keywords:** bimetallic acetates · heterogeneous catalysis · photoelectron spectroscopy · structure elucidation

## Introduction

Supported palladium catalysts play an important role in organic synthesis.[1–4] Palladium acetate serves as a chloride-free precursor for catalysts used in hydrogenation and partial oxidation of olefins,[5–7] but one disadvantage of its use in catalyst preparation is its poor solubility in polar solvents. The crystal structure of palladium acetate was determined by Skapski and Smart in 1970 and re-investigated in 1993.[8, 9]

Palladium acetate forms a trimer in the solid state.[8, 9] Relevant geometric parameters of palladium acetate and cadmium acetate are given in Table 1. Three palladium atoms are connected by bridging bidentate acetate groups. Each palladium atom attains a square-planar coordination, which is usually of low energy for $d^8$ elements. The chelating effect of bridging acetate groups is responsible for additional stabilisation.

Table 1. Selected bond lengths [pm] and angles [°] of $[Pd(CH_3COO)_2]_3$[8,9] and $Cd(CH_3COO)_2 \cdot 2H_2O$.[11]

| $[Pd(CH_3COO)_2]_3$ | | $Cd(CH_3COO)_2 \cdot 2H_2O$ | |
|---|---|---|---|
| Pd–Pd | 310.5–320.3(1) | | |
| Pd–O | 197.3–201.4(1) | Cd–O | 229.7–259.7(3) |
| Pd-O-C | 127.8–133.2(8) | Cd-O-C | 86.9–122.3(5) |
| O-C-O | 124.8–128.7(11) | O-C-O | 118.0–122.3(5) |

The solubility of palladium acetate increases immediately when cadmium acetate is added; clear orange solutions are obtained. Two explanations may account for this effect. The solubility may increase because the additional acetate ions act as an isoionic additive. In this case other metal acetates should produce the same effect. Another cause may be the complex chemistry of palladium(II) and cadmium(II) in solution. Indeed, we were able to isolate a crystalline solid from stoichiometric Pd acetate/Cd acetate solutions. Solutions with Na acetate or K acetate resulted in neither an increased solubility nor complex formation.

It is well known from the literature that Pd and Cd form alloys;[24, 25] a possible Cd promoter effect may be traced back to such alloy formation, but it may be due to an electronic or

[*] Prof. Dr. R. Schlögl, Dr. G. Mestl, Dr. S. Adam, O. Timpe, U. Wild
Fritz-Haber-Institut der Max-Planck-Gesellschaft
Abteilung Anorganische Chemie
Faradayweg 4–6, D-14195 Berlin (Germany)
Fax: (+49) 30 84134401
E-mail: robert@graphite.rz-berlin.mpg.de
Prof. Dr. W. Bensch
Institut für Anorganische Chemie der Universität Kiel
Olshausenstr. 40, D-24118 Kiel (Germany)



0947-6539/98/0408-1458 $ 17.50+.50/0 *Chem. Eur. J.* **1998**, *4*, No. 8

steric effect of Cd on the active Pd species. The modification of the precursor through the formation of a Pd–Cd complex before adsorption onto the support may thus have a crucial influence in the generation of the catalytically active Pd species.

To establish the effect of the precursor modification on the catalytic performance, the activation of the precursor to form the active Pd catalyst has been characterised in detail. Furthermore, it has been shown that the molecular structure of the precursor is preserved upon immobilisation on the support. Finally, a model catalytic reaction has been used to illustrate the differences in performance of catalysts prepared from Pd acetate and from the newly isolated complex.

## Results

**The unsupported Pd–Cd complex:** A microcrystalline substance was obtained from a saturated solution of palladium acetate and cadmium acetate in glacial acetic acid. Recrystallisation from acetic acid yielded rectangular single crystals of suitable size and quality for X-ray structure analysis, which were stable in air at room temperature. Details of the structure determination are listed in Tables 2 and 3. The geometric structure of the complex is shown in Figure 1. Palladium is surrounded by four bridging bidentate acetate ligands, forming a square. Cadmium is coordinated by six

Table 2. Crystal and structural data of $[CdPd(CH_3COO)_4 \cdot CH_3COOH]_2$.

| | |
|---|---|
| formula | $[CdPd(CH_3COO)_4 \cdot CH_3COOH]_2$ |
| crystal size | $0.50 \times 0.32 \times 0.14$ mm |
| crystal system | triclinic |
| space group | $P\bar{1}$ |
| $Z$ | 1 |
| $a$ [pm] | 855.2(1) |
| $b$ [pm] | 899.0(1) |
| c [pm] | 1071.2(2) |
| $\alpha$ [°] | 82.231(6) |
| $\beta$ [°] | 74.230(5) |
| $\gamma$ [°] | 76.429(5)° |
| calculated density [g cm$^{-3}$] | 2.226 |
| wavelength [pm] | $Mo_{K\alpha}$ $\lambda = 71.073$ |
| temperature [K] | $150 \pm 0.5$ |
| area | $3° \leq 2\theta \leq 60°$ |
| reflections | 4726 measured, 4442 independent |
| absorption | numeric correction, $\mu = 2.60$ mm$^{-1}$ |

Table 3. Selected bond lengths [pm] and angles [°] with standard deviations in parentheses.[28]

| | | | | | |
|---|---|---|---|---|---|
| Cd–O2 | 235.2(2) | O9-Cd-O3a | 133.74(7) | O9-Cd-O5 | 84.29(8) |
| Cd–O3 | 231.4(2) | O3a-Cd-O5 | 79.01(7) | O9-Cd-O3 | 146.51(7) |
| Cd–O3[a] | 229.2(2) | O3a-Cd-O3 | 74.17(7) | O5-Cd-O3 | 84.39(7) |
| Cd–O5 | 230.3(2) | O9-Cd-O2 | 88.51(8) | O3a-Cd-O2 | 76.77(7) |
| Cd–O7 | 240.2(2) | O5-Cd-O2 | 138.31(7) | O3-Cd-O2 | 120.06(8) |
| Cd–O9 | 222.5(2) | O9-Cd-O7 | 86.68(7) | O3a-Cd-O7 | 130.29(7) |
| Cd–Pd | 280.58(4) | O5-Cd-O7 | 142.83(7) | O3-Cd-O7 | 83.59(7) |
| Pd–O4 | 200.7(2) | O6-Pd-O8 | 174.77(8) | O6-Pd-O4 | 91.12(8) |
| Pd–O6 | 197.8(2) | O8-Pd-O10 | 90.48(8) | O10-Pd-O4 | 178.82(8) |
| Pd–O8 | 199.7(2) | O8-Pd-O4 | 88.41(8) | | |
| Pd–O10 | 200.0(2) | | | O6-Pd-O10 | 89.95(8) |

[a] a denotes symmetry operation $-x, -y+1, -z$.

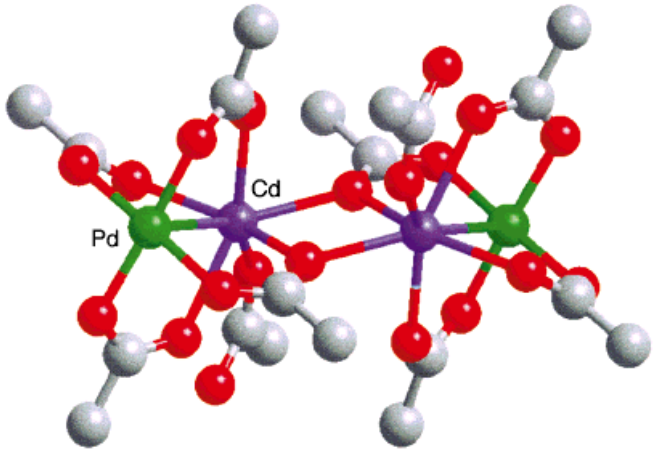


Figure 1. Crystal structure of $[CdPd(CH_3COO)_4 \cdot CH_3COOH]_2$, Cirius[2] plot.

acetate ligands (one of which is the solvating acetic acid) in trigonal-prismatic geometry. This is an unusual coordination for cadmium(II), for which octahedral arrangements are more common.[10] One acetate ligand is unidentate (bound acetic acid), whereas the other three acetate ligands bridge palladium and cadmium. Two cadmium atoms of a monomeric unit are linked by two acetate ligands. The Cd–O distances of the chelating ligands vary in the region of 230 pm; the longest Cd–O distance of 235.2(2) pm is observed for the weakly bound acetic acid molecule (Cd–O2; see Table 3). Palladium, as the seventh ligand, caps a rectangular plane of the prism. The only known cadmium compound with a coordination number of seven is $Cd(CH_3COO)_2 \cdot 2H_2O$.[11] The distance between palladium and cadmium (280 pm) is much less than the sum of the van der Waals radii (320 pm). Short metal–metal bond lengths are also observed in other acetate compounds, for example dimeric copper acetate (Cu–Cu 264 pm).[12] The observed Pd–O and Cd–O bond lengths are very similar to the distances in the binary substances. The coordination polyhedra of the parent compounds, however, exhibit significant distortions, as reflected in expanded bond angles.[8]

The room-temperature $^{13}C$ NMR spectrum of the binuclear compound dissolved in $D_2O$ (spectra not shown) had two peaks at $\delta = 31.030$ and 22.295 for chemically nonequivalent methyl groups. The additional peaks at $\delta = 216.210$ and 179.692 were assigned to the respective carboxyl groups. The pair of signals at relatively low chemical shifts indicated the existence of weakly bound unidentate ligands such as solvating acetic acid. The other set of signals represents all the acetate ligands bridging the metal centres (either palladium–cadmium or cadmium–cadmium).

$^{113}Cd$ NMR measurements (spectra not shown) indicated that cadmium was bound as a divalent cation in the binuclear complex. Pure $Cd(OAc)_2$ shifts to $\delta = 18.56$ relative to the perchlorate standard. The cadmium tetraacetatopalladate acetate dissolved in $D_2O$ had a single peak at $\delta = 17.66$.

A combined instrument for thermogravimetry (TG), differential thermal analysis and on-line gas analysis was used to characterise the thermal stability of the ternary precursor in a nitrogen atmosphere. Figures 2 and 3 display the results of this

  0947-6539/98/0408-1459 $ 17.50+.25/0 

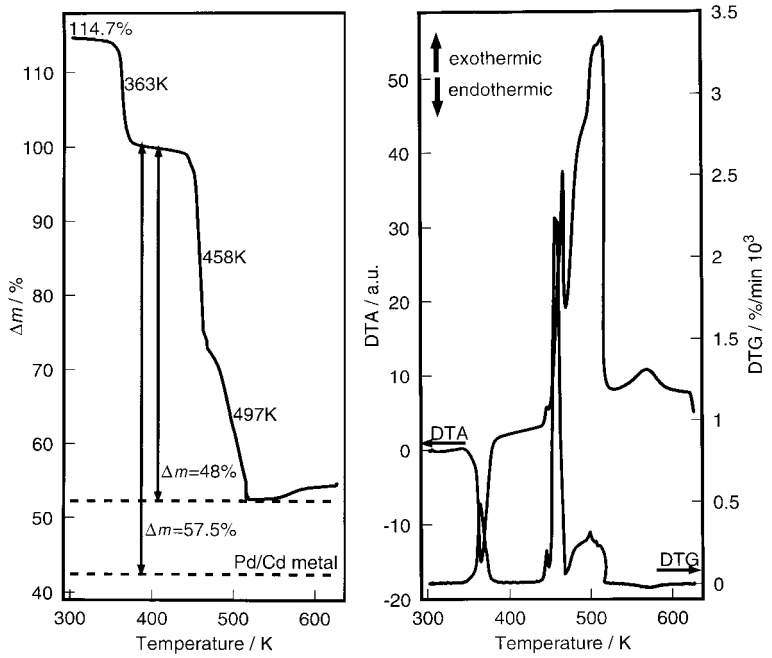


Figure 2. Thermal decomposition of $[CdPd(CH_3COO)_4 \cdot CH_3COOH]_2$ under a nitrogen atmosphere (82.2 mL min$^{-1}$), heating rate 5 K min$^{-1}$, $m_E = 10.29$ mg. Left: TG curve; right: DTA and DTG curves.

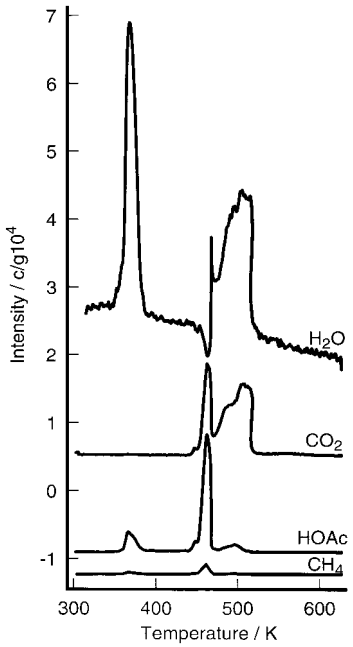


Figure 3. IMR-MS spectra of detected decomposition products. The data are uncorrected for the IMR-MS cross-sections. The intensity of the acetic acid curve was corrected for the sensitivity of the IMR-MS machine. Heating rate 5 K min$^{-1}$.

thermal activation. Three main events at 363, 458 and 497 K were detected in the weight loss curve for the thermal decomposition of the precursor compound (Figure 2). Analysis (IMR-MS traces) of the evolved gases (Figure 3) showed that the first weight loss was due to water evolution and the desorption of weakly solvating acetic acid, which was also detected by NMR spectroscopy, and this loss was not characteristic of the decomposition of the binuclear complex. For this reason, the 100% line in the TG analysis (see Figure 2 left) was positioned at the first plateau above 363 K. The observed maximum weight loss of 48% was incompatible with the abstraction of all intact ligands. A complete ligand abstraction would require a total weight loss of 57.5%.

From the DTA profile in Figure 2 right it was deduced that all three events were multiple processes, as revealed by the split or broadened peaks. The DTA curve indicated that the low-temperature water evolution was an endothermic process, whereas the ligand abstraction steps at higher temperatures were strongly exothermic reactions. The unchanged heat capacity evident in the DTA trace after the first endothermic water/acetic acid evolution indicated that desorbed water and acetic acid were extramolecular entities.

The first decomposition step of the stoichiometric solid at 458 K comprised the abstraction of acetate ligands in the form of acetic acid and its decomposition products, $CH_4$ and $CO_2$. In an inert gas atmosphere, a second decomposition step that was observed at about 40 K above the main one occurred on a different reaction pathway, as evidenced by the reaction products that were detected ($CO_2$ and water), together with the overall exothermicity of the process. $CH_4$ was not detected during this final decomposition stage. A minor additional reaction event occurred at about 570 K. The exothermic process terminated with the evolution of very small amounts of $CO_2$. A weight increase of about 1% which appeared to end at 650 K was detected.

The thermal decomposition of the complex was also studied with the surface-sensitive method XPS. This method requires careful determination of the binding-energy scale for isolated samples such as the present complex. In addition, X-ray-induced damage may lead to erroneous reduction temperatures. The change in intensity of the photoemission peaks with irradiation time was monitored. The unsupported Pd complex did not seem to be susceptible to complete irradiation damage, as proved in an independent series of experiments (data not shown), in contrast to published reports concerning supported Pd acetates.[13, 14] Pd acetate is decomposed and reduced to Pd under X-ray irradiation.

The carbon 1s data for a decomposition reaction sequence are shown in Figure 4. Up to 423 K, the XP spectra consisted of two lines of equal intensity, characteristic of methyl carbon at 285 eV and of carboxyl carbon at 288.6 eV. The integrity of the sample was indicated by the expected 1:1 intensity ratio in the spectra. After treatment at 423 K, the C 1s signal intensity had already decreased to 80% of the initial value; this confirmed an initial decomposition. At 473 K, above the temperature at which the first weight loss occurred in the TG data (458 K; see Figure 2 left), the total C 1s XPS intensity was reduced to about 50% of the initial value, and the signals also showed a pronounced broadening. After treatment at 523 K, at which temperature the decomposition had already terminated according to TG data, carboxylic carbon (289 eV) was still detected at an intensity that had been further reduced to 40% of the initial value. The intensity of the aliphatic C 1s signal at 285 eV, however, was increased after this treatment. After annealing of the sample at 573 K, the aliphatic C 1s signal at 285 eV was further increased in intensity, but carboxylic species were detected only as a weak shoulder at about 288 eV.

This sequence of events could be further substantiated by analysis of the metal spectra displayed in Figures 5 left and 5



0947-6539/98/0408-1460 $ 17.50+.50/0 *Chem. Eur. J.* **1998**, *4*, No. 8

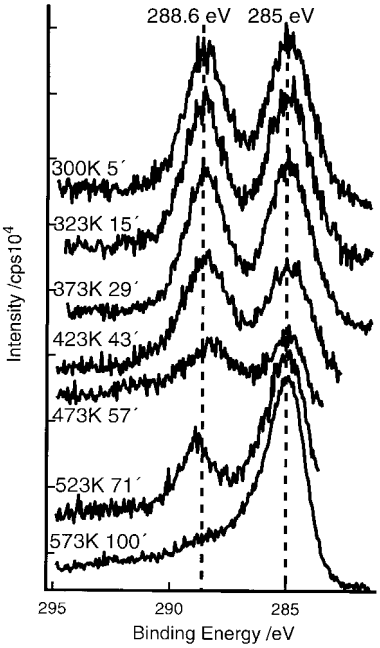


Figure 4. C 1s XP spectra of $[CdPd(CH_3COO)_4 \cdot CH_3COOH]_2$ during thermal decomposition. The time data indicate the duration of the total X-ray irradiation. Each temperature window was kept constant for 30 min before the spectra were recorded. The spectra are shifted vertically for clarity.

right. The Pd 3d spectra in Figure 5 left, recorded at room temperature after treatment at 323 and 373 K, revealed the presence of divalent Pd. At 423 K, most of the Pd was reduced to the element, with the expected binding energy of 335.5 eV.[15, 16] The broadening at higher binding energies was evidence that some unreduced Pd remained in the sample. This may explain why the total C 1s signal intensity had not decreased by 50% after this treatment step, as one would expect from the Pd reduction. At the same time, the Pd 3d signal integral intensity was reduced to 60% of the initial value.

A considerable sharpening of the peak profile of the Pd 3d signal was observed after heat treatment at 473 K, together with a further reduction of the Pd 3d intensity to 35% of the initial value. After the treatment at 523 K, the intensity of the Pd 3d signal further decreased to about 30% and finally, after treatment at 573 K, to 20% of the initial value. During this process, the Pd 3d signal continuously shifted to higher binding energies, and the full widths at half maximum (FWHMs) decreased from 2.02 to 1.23 eV. The intensity reduction and the sharpening of the FWHM were evidence for Pd particle sintering. Interestingly, the Pd $3d_{5/2}$ to $3d_{3/2}$ intensity ratios were considerably different from the theoretical value of 1.6 (see Table 4), and were especially low after treatment at 423 and 473 K. This was additional proof of the presence of at least two different Pd species during the first decomposition step.

Table 4. XPS characteristics of the Pd 3d signals of $[CdPd(CH_3COO)_4 \cdot CH_3COOH]_2$ during the thermal treatment.

| Temperature [K] | BE Pd $3d_{5/2}$ eV[a,b] | Intensity 5/2 cps | Intensity 3/2 cps | Intensity ratio 5/2:3/2 | FWHM 5/2 [eV] |
|---|---|---|---|---|---|
| 300 | 338.5 | $1.788 \times 10^6$ | $1.400 \times 10^6$ | 1.277 | 1.87 |
| 323 | 338.5 | $1.705 \times 10^6$ | $1.386 \times 10^6$ | 1.230 | 2.02 |
| 373 | 338.5 | $1.648 \times 10^6$ | $1.372 \times 10^6$ | 1.201 | 2.02 |
| 423 | 335.5 | $1.049 \times 10^6$ | $1.271 \times 10^6$ | 0.825 | 1.95 |
| 473 | 335.8 | $6.082 \times 10^5$ | $7.993 \times 10^5$ | 0.761 | 1.37 |
| 523 | 336.4 | $4.184 \times 10^5$ | $3.713 \times 10^5$ | 1.127 | 1.30 |
| 573 | 336.4 | $2.333 \times 10^5$ | $2.397 \times 10^5$ | 0.973 | 1.23 |

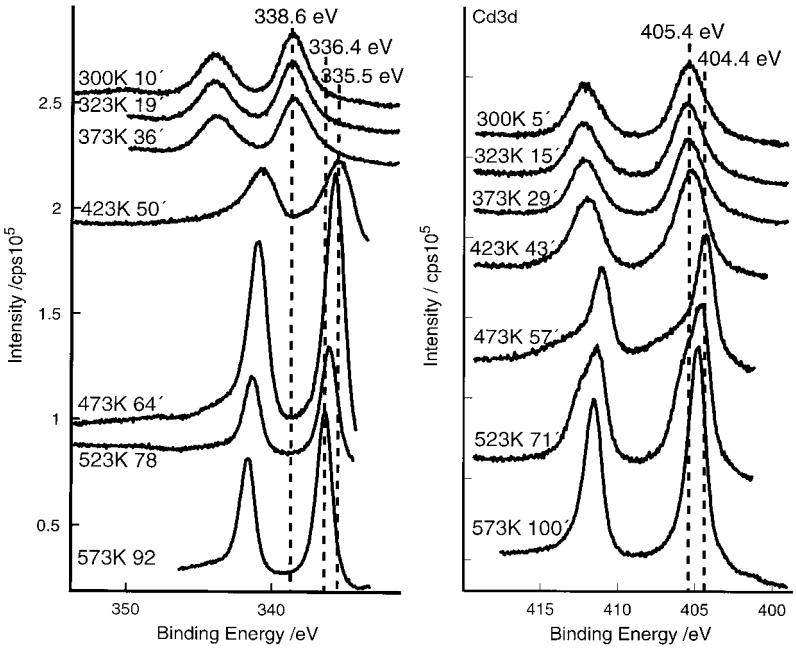


Figure 5. XP spectra of $[CdPd(CH_3COO)_4 \cdot CH_3COOH]_2$ during thermal decomposition: a) Pd 3d signals; b) Cd 3d signals. The spectra are shifted vertically for clarity.

It is highly relevant (Figure 5 right) that the Cd species was still present in its divalent form at 423 K. The Cd acetate was significantly decomposed to elemental Cd only after annealing at 473 K, as evidenced by the binding energy of 404.4 eV.[14] The broad shoulder at about 406 eV indicating the presence of some ill-defined $Cd(OAc)_2$ was consistent with the C 1s spectrum, which showed that some carboxylates remained. After heat treatment at 523 K, Cd metal and $Cd(OAc)_2$ were indicated by the signal at 404.5 eV with a shoulder at 405.7 eV. This high-energy shoulder could not be attributed to differential charging because such shoulders were not observed in the signals of the other elements. The sharpening of the shoulder at 405.7 eV was evidence that the $Cd(OAc)_2$ species was much better defined after annealing at 523 K than at 473 K. At 573 K Cd was reoxidised, as indicated by the shift of the Cd 3d signal to higher binding energies, while the high-energy shoulder due to $Cd(OAc)_2$ at 405.7 eV was completely lost.

This spectrum was therefore attributed solely to the presence of cadmium oxide. The Cd 3d signal intensity was gradually reduced during this whole process. The strongest intensity reduction, from 75 to 30% of the initial value, occurred after the treatments at 523 and 573 K. The aliphatic C 1s signal intensity grew after the treatments at 523 and 573 K, from 45 to 70% of the initial value. The decrease in the intensities of the O 1s and Pd 3d XPS signals after the treatments at 523 and 573 K correlated neither directly with the decrease in the Cd 3d XPS signal intensity, nor inversely with the increase in the aliphatic C 1s XPS signal intensity.

Figure 6 shows the intensities of the Pd 3d and Cd 3d XPS signals after correction by atomic sensitivity factors (ASF) and normalisation. At temperatures above 375 K, the XPS signal

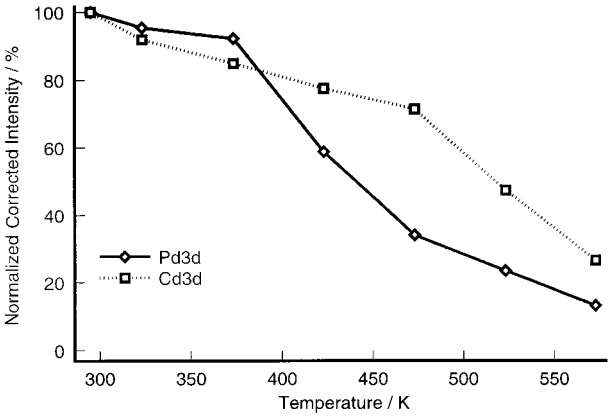


Figure 6. ASF-corrected XPS intensities of Pd 3d and Cd 3d signals normalised to the initial intensity, as a function of the temperature.

intensity of Pd decreased while that of Cd remained at a higher higher level. These changing XPS intensities are clear evidence that the Pd species sintered into small particles, while Cd remained more homogeneously distributed throughout the sample.

The IR bands observed and peak assignments[20, 21, 23] for crystalline solid $[CdPd(CH_3COO)_4 \cdot CH_3COOH]_2$ are listed in Table 5. The spectrum at 298 K shows two sets of bands which are caused by strongly bound acetate ligands and solvated acetic acid molecules, as shown in Figure 7. The two combination modes of the deformation $\delta(CO_2)$ and $CH_3$ rocking modes resulted in IR bands at 1697 and 1667 $cm^{-1}$ with an intensity ratio of 4:1. The broad band at 1668 $cm^{-1}$

Table 5. Vibrational frequencies of $[CdPd(CH_3COO)_4 \cdot CH_3COOH]_2$.

| Bands [$cm^{-1}$] | Assignment |
|---|---|
| 1697 | DRIFT |
| Combination $\delta$(COO) and $CH_3$ rocking | |
| 1665 | DRIFT |
| Combination $\delta$(COO) and $CH_3$ rocking | |
| 1549 | DRIFT $\nu(CO_2)$ antisymmetric |
| 1533 | DRIFT $\nu(CO_2)$ antisymmetric |
| 1466 | DRIFT $\nu(CO_2)$ symmetric |
| 1456 | DRIFT $\nu(CO_2)$ symmetric |
| 1405 | DRIFT $\delta(CH_3)$ |
| 1354 | DRIFT $\delta(CH_3)$ |
| 1319 | DRIFT $\delta(CH_3)$ |
| 1255 | DRIFT $\delta(CH_3)$ |

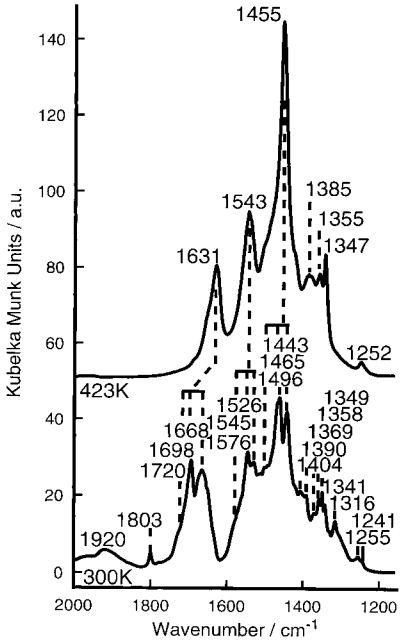


Figure 7. DRIFTS spectra of $[CdPd(CH_3COO)_4 \cdot CH_3COOH]_2$ at room temperature and at 423 K. Spectra are shifted vertically for clarity.

is assigned to the four bidentately bound acetate groups per formula unit, which differ in their bridging functions (see Table 2). The sharp band at 1698 $cm^{-1}$ is attributed to the unidentately bound acetic acid molecule. One set of IR bands disappeared after treatment at 423 K because of the desorption of acetic acid, in agreement with the TG and NMR investigations. The spectrum of the unsolvated binuclear complex was observed after treatment at 423 K.

IR spectroscopic investigations of interactions of carboxylates with various organic compounds were reported previously.[17] Brandon and Claridge investigated heteronuclear acetate-bridged complexes, including mixtures of palladium acetate with various bivalent metal acetates in acetic acid, by IR and UV/Vis spectroscopy.[23] They reported complexes with bridging acetate groups, on the basis of their IR spectra. The differences in symmetric and antisymmetric $CO_2^-$ vibrational frequencies have been compared with the value observed for sodium acetate.[18–20] When the difference is lower than 165 $cm^{-1}$ bridging or chelating acetate groups are expected, whereas for differences of more than 200 $cm^{-1}$ the acetate should be unidentate.[21] Although such discrimination did not remain uncriticised,[22] this rule has now been confirmed in the case of $[CdPd(CH_3COO)_4 \cdot CH_3COOH]_2$. The difference in wavenumbers, $\nu = 92$ $cm^{-1}$, between the antisymmetric (1545 $cm^{-1}$) and symmetric (1443 $cm^{-1}$) $CO_2^-$ stretching frequencies demonstrated the existence of bridging or chelating acetate ligands, in line with the X-ray structure determination.

The unidentately bound acetic acid molecule was detectable by means of a shoulder at 1576 $cm^{-1}$ due to the antisymmetric $CO_2$ vibration ($\nu = 168$ $cm^{-1}$). After treatment at 573 K intact Pd–Cd complexes could no longer be observed.



0947-6539/98/0408-1462 $ 17.50+.50/0 *Chem. Eur. J.* **1998**, *4*, No. 8

**Silica-supported Pd–Cd complex**: In order to substantiate the effect of Cd addition on the catalytic performance, it is essential to show how the ternary precursor is bound to the substrate. UV/Vis spectroscopy was used to follow the evolution of the molecular Pd–Cd precursor during impregnation of the catalyst. The relevant data are shown in Figure 8. The absorption maximum due to the charge transfer between Pd and oxygen was detected at 396 nm for pure palladium acetate in acid solution (spectrum a, Figure 8A).[23] The UV/Vis spectrum of $[CdPd(CH_3COO)_4 \cdot CH_3COOH]_2$ in acid solution (pH 1) showed this maximum absorption at 343 nm (spectrum b, Figure 8A) due to the less distorted Pd coordination. After impregnation of an $SiO_2$ support with the Cd–Pd complex, we observed an absorption maximum at 340 nm together with a shoulder at about 400 nm for the dried solid (spectrum a, Figure 8B), at the same wavelength as the absorption maximum of binary palladium acetate (spectrum b, Figure 8B), indicating that the complex was not adsorbed entirely intact onto silica.

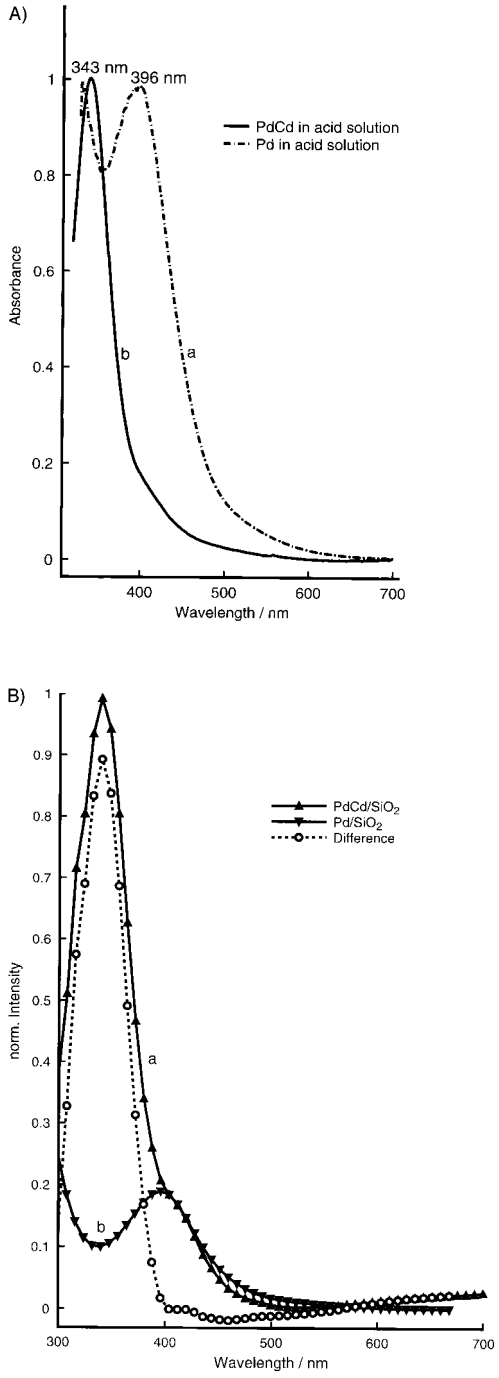


Figure 8. A) UV/Vis spectra of a) $[Pd(OAc)_2]_3$ and b) $[CdPd(CH_3COO)_4 \cdot CH_3COOH]_2$ in acid solutions and as crystalline solids. Spectra are shifted vertically for clarity. B) UV/Vis spectra of a) $[CdPd(CH_3COO)_4 \cdot CH_3COOH]_2$ and b) $[Pd(OAc)_2]_3$ supported on $SiO_2$. Broken line: difference spectrum of a) minus 20% of b). Spectra are normalised for quantification.

Comparison of the DRIFTS spectrum of the pure Pd–Cd complex as a crystalline solid with that of the Pd–Cd complex adsorbed on $SiO_2$ revealed that they were completely different (Figure 9), especially in that the bands at 1545, 1454, 1383 and 1246 $cm^{-1}$ (Figure 9, spectrum c), which are characteristic of the Pd–Cd complex, could not be detected for the adsorbed species. A further comparison with the spectrum of $CH_3COOH$ on $SiO_2$ (Figure 9, spectrum a) showed some similarity in both spectra. Most of the spectral features that were detected presumably arose from adsorbed acetic acid. However, signal intensity ratios, for example the band at 1732 $cm^{-1}$, differed and there were two bands/shoulders in the spectrum of the adsorbed Pd–Cd complex (Figure 9, spectrum b) at 1570 and 1297 $cm^{-1}$ which were absent in the spectrum of acetic acid on $SiO_2$ (Figure 9, spectrum a). This complete difference between the DRIFTS spectrum of the adsorbed complex and that of the pure compound confirms the DR-UV/Vis results and suggested that the complex was at least partially decomposed upon adsorption onto $SiO_2$.

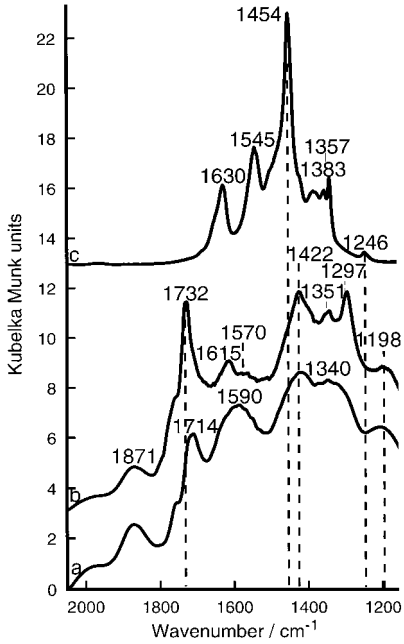


Figure 9. DRIFT spectra of $CH_3COOH$ on $SiO_2$, and of $CdPd(CH_3COO)_4 \cdot CH_3COOH]_2$ supported on $SiO_2$ and as a crystalline solid at 423 K. Spectra are shifted vertically for clarity.

For the supported precursor compound and the pure precursor crystals, the Pd 3d XPS spectra before activation are shown in Figure 10. At room temperature, the binding

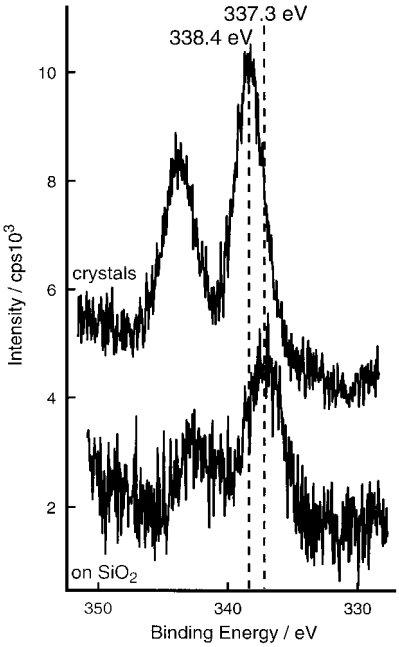


Figure 10. XP Pd 3d spectra of $[CdPd(CH_3COO)_4 \cdot CH_3COOH]_2$ supported on $SiO_2$ and as a crystalline solid at room temperature. Spectra are shifted vertically for clarity.

energy of the $SiO_2$-supported cluster was observed at 337.3 eV (referenced to the aliphatic C 1s signal at 285 eV). The Pd 3d signal of the unsupported material, however, was at 338.4 eV. In addition, the Pd $3d_{5/2}$ to $3d_{3/2}$ intensity ratio of the supported cluster was 1.9, whereas that of the unsupported material was 1.5, which is close to the theoretical value. The shift of about 1 eV in the binding energy of the supported material relative to the unsupported cluster indicated decomposition of the cluster and formation of oxidic Pd surface species (see Table 4). This XPS finding was in accord with the DR-UV/Vis and DRIFTS observations of a partial decomposition of the Pd – Cd complex upon adsorption onto $SiO_2$.

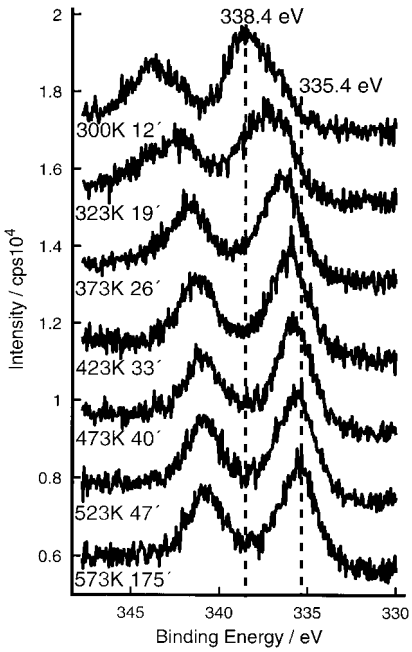


Figure 11. XP Pd 3d spectra of $SiO_2$-supported $[CdPd(CH_3COO)_4 \cdot CH_3COOH]_2$ during thermal decomposition. Spectra are shifted vertically for clarity.

Complete decomposition of the supported complex to elemental Pd was observed after thermal decomposition in ultrahigh vacuum (UHV) (Figure 11). However, in contrast with the unsupported complex, it was detected only after heat treatment at 573 K. This very important result indicated that the stability of the complex towards reduction changed after adsorption and interaction with the support.

TEM images of the black catalysts after oxidation of ethylene are displayed in Figure 12. The particulate metals detected by TEM in the two catalysts that were investigated differed greatly in particle size and particle size distribution. The decomposition of the binary palladium acetate precursor generally led to agglomerated particles, as shown in Figure 12 top. Very few isolated particles were found that were as small as 5 nm. Figure 12 bottom shows the highly dispersed particles

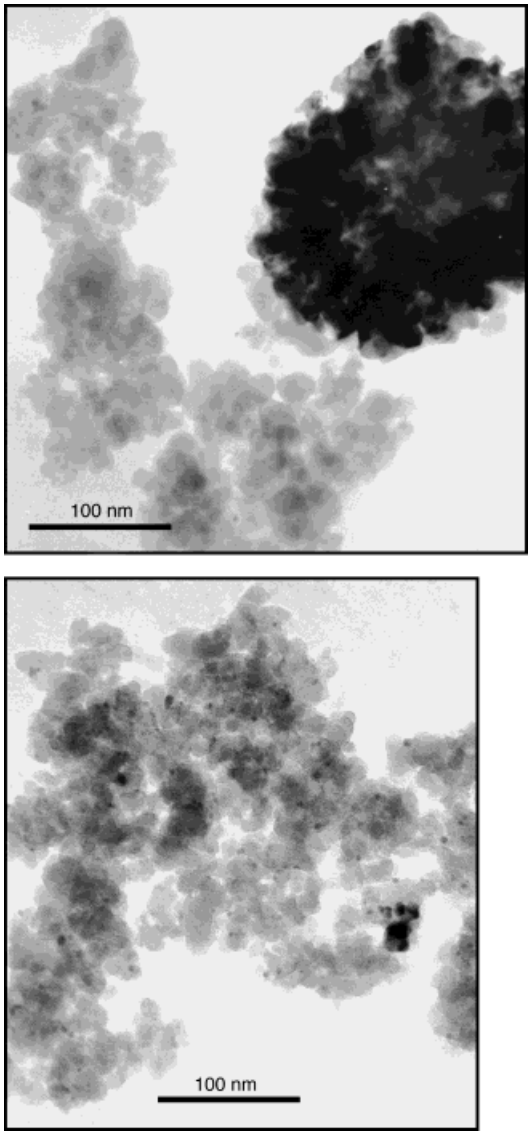


Figure 12. TEM micrographs spectra of a) $[Pd(CH_3COO)_2]_3$ and b) $[CdPd(CH_3COO)_4 \cdot CH_3COOH]_2$ on $SiO_2$ after the IMR-MS investigations.



0947-6539/98/0408-1464 $ 17.50+.50/0 *Chem. Eur. J.* **1998**, *4*, No. 8

obtained from the Pd–Cd precursor. Particles of the isolated Pd clusters varied in size around 2 nm, and were therefore somewhat smaller than the smallest particles formed from the binary palladium acetate precursor.

We chose the total oxidation of ethylene to test the activity of catalysts derived from the ternary precursor $[CdPd(CH_3COO)_4 \cdot CH_3COOH]_2$ in comparison with a catalyst made from the conventional binary precursor $[Pd(CH_3COO)_2]_3$. $SiO_2$ supports (BET surface area 159 $m^2 g^{-1}$) were impregnated with solutions of each compound in glacial acetic acid and dried under vacuum. The BET surface areas were 133 and 130 $m^2 g^{-1}$ for supported Pd acetate and Pd–Cd acetate, respectively, after these pretreatment steps. The samples were activated by heating them in flowing $N_2$ to 425 K in order to decompose the acetate ligands. This process was monitored through the evolution of fragments of $m/z$ 44. The formation of $CH_4$ as a fragmentation product of acetic acid was detected for both catalysts (data not shown).

At 425 K, a flow of ethylene and a small flow of oxygen were added, while the sample was being heated to 573 K. The results of the conversion are discussed in light of the IMR-MS responses, which are presented for $CO_2$ and for $CH_4$ in Figure 13. $H_2O$ formation was found to follow the $CO_2$ profile exactly, and therefore it is not shown.

The formation of $CO_2$ started over both samples at 473 K (Figure 13A), indicating a similar activity with respect to the light-off temperature. With respect to the amount of $CO_2$ produced, the two catalyst materials showed very different behaviour. The $CO_2$ intensity increased for the Pd–Cd/$SiO_2$ sample in a stepwise fashion, in contrast to the Pd/$SiO_2$ sample, for which a monotonic increase was observed. Keeping the temperature of the reactor at 573 K for 30 min resulted in a massive decrease in $CO_2$ evolution for Pd–Cd/$SiO_2$ (Figure 13A, inset) The pure Pd/$SiO_2$ catalyst formed $CO_2$ continuously, even after the reactor had been cooled to 523 K (Figure 13B). Figure 13C shows $CO_2$ formation during a second period of heating to 573 K. The Pd–Cd/$SiO_2$ catalyst again formed large amounts of $CO_2$, in contrast to the Pd/$SiO_2$ sample, which was completely inactive during the second heating cycle.

## Discussion

**The unsupported Pd–Cd complex**: The short metal–metal distance in the Pd–Cd complex may suggest an interaction between Pd and Cd. $^{113}Cd$ NMR spectroscopy revealed that pure $Cd(OAc)_2$ shifted to $\delta = 18.56$ relative to the perchlorate standard, whereas cadmium tetraacetatopalladate showed a single peak at $\delta = 17.66$. The shift relative to the binary compound was probably induced by $Pd^{2+}$ in the close neighbourhood. However, the cationic bonding of the Cd centre as revealed by NMR spectroscopy is a strong indication of the absence of a chemical bond between Cd and Pd, despite the short crystallographic interatomic distance. In addition, XPS revealed that both metals were in their divalent state. A metallic bond can thus be excluded. It is thought more likely that the short metal–metal distance results from compression of the nonbonding metal centres by the chelating ligands.

It may be concluded that, because of the short metal–metal distances in $[CdPd(CH_3COO)_4 \cdot CH_3COOH]_2$, a Pd–Cd alloy phase, such as reported by Nowotny and co-workers, results from activation at higher temperatures and acetate ligand decomposition.[24, 25] Differential scanning calorimetry measurements (data not shown) did not reveal any effect in the decomposition temperature interval compatible with formation of an alloy. In addition, no powder X-ray diffraction

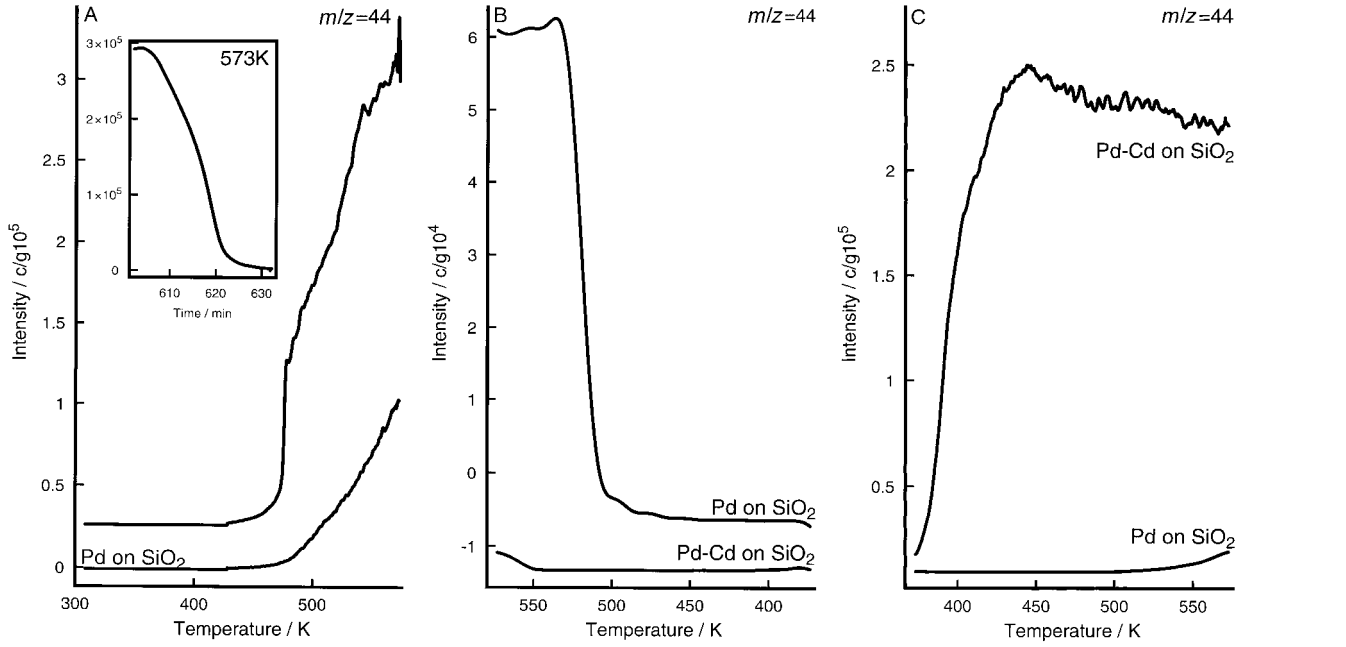


Figure 13. IMR-MS spectrum of the oxidation of ethylene with $[Pd(CH_3COO)_2]_3$ and $[CdPd(CH_3COO)_4 \cdot CH_3COOH]_2$ on $SiO_2$. A) Formation of $CO_2$ in the temperature range 308–573 K (heating rate 0.5 K $min^{-1}$). B) Formation of $CO_2$ in the temperature range 573–373 K (cooling rate 5 K $min^{-1}$). C) Formation of $CO_2$ in the temperature range 373–573 K (heating rate 5 K $min^{-1}$).

evidence was found to support the existence of alloy particles with dimensions larger than 0.5 nm. Furthermore, from XPS intensity considerations (Figure 6), we may conclude that Pd is sintered into particles, whereas the Cd species remains more homogeneously distributed after thermal decomposition. Formation of an alloy between Pd and Cd under these conditions is therefore excluded; the observed Cd promoter effect cannot arise from such a process.

The interpretation of the mass spectra in the present form is only possible because the IMR-MS technique produces signals from the molecules described without fragmentation reactions. Therefore any decomposition of acetic acid is not a consequence of the ionisation but occurs during decomposition of the solid. The results in Figures 2 and 3 show that complete ligand abstraction is a complex process. It is incomplete in the sense that metallic Pd and Cd are not obtained, as has been proved independently by XPS.

Desorption of water and acetic acid was detected at 370 K. Weakly coordinated acetates were detected by solution NMR spectroscopy. Therefore, it is concluded that the dissolved solid contained additional acetic acid to the nominal stoichiometry determined from the X-ray structure. This is completely in accord with the observations in the TG/TDA-IMR-MS experiment.

The first stage of decomposition of the complex at 460 K yields acetic acid, methane and $CO_2$, indicating that a cleavage of the ligand molecules occurs during decomposition. The simultaneous ligand abstraction together with the cleavage of the C – C bonds occurs very rapidly, as is seen from the sharp peaks in Figures 2 and 3.

Complete ligand abstraction requires a second step in an inert gas atmosphere at about 40 K above the main decomposition reaction. As Figure 3 shows, the absence of water of hydration and the higher reaction temperature seem to result in a different reaction path from that of the first decomposition step. The presence of reaction products $CO_2$ and water in the absence of gas-phase oxygen, together with the overall exothermicity of the process, indicates that additional reactions must also take place which do not form gas-phase products and that consume carbon. The formation of carbonaceous deposits on $Pd^0$ is a probable reaction and is proved to occur by the strong increase of the C 1s XPS signal. Carbon may also be dissolved in metallic Pd to form an interstitial compound, as shown by McCauley.[24]

A minor additional reaction event occurred at about 570 K. The exothermic process terminated with the evolution of very small amounts of carbon dioxide. In addition, a weight increase of about 1% was detected which appeared to end at 650 K. The carbon dioxide evolution between 495 K and approximately 570 K may be explained by the decomposition of the remaining carboxylic species which was detected by XPS. The weight increase of 1% which terminated at 650 K may be attributed to the oxidation of Pd species by the residual oxygen impurities (< 5 ppm) in the carrier gas, nitrogen.

The integrity of the sample during the heat treatment to 423 K is confirmed by the detection of the expected 1:1 intensity ratio of the aliphatic and carboxylic C 1s XPS signals (Figure 4). The successive broadening of the C 1s, Pd 3d and Cd 3d lines with a further increase in temperature to 375 K indicates differential charging effects which arise from the desorption of $H_2O$ and acetic acid. This desorption is evident from the observed decrease in the FWHM of the O 1s signal and by the TG experiment. A significant loss of the total C 1s intensity is observed in the XPS spectra after treatment at 473 K (Figure 4). The FWHMs of all elements, except oxygen, decrease at the same time. Additionally, the binding energy of the O 1s signal shifts to higher energies while the signal intensity decreases. These combined effects are evidence for the decomposition of the Pd – Cd complex. The reduction in the FWHM of all elements except O can be explained by the formation of metallic Pd, as shown by the low binding energy of this signal (Figure 5 left). At 523 K, we still observed the presence of residual carboxylic carbon together with an initial surface segregation of carbon, as demonstrated by the increased intensity of the C 1s signal at 285 eV (Figure 4). This species originates from carbonaceous deposits, the existence of which is also deduced from the decomposition products detected in the TG/TDA – IMR-MS experiment.

The Pd 3d spectra in Figure 5 left, recorded at room temperature after treatment at 323 K and 373 K, revealed the presence of divalent Pd. Their tailing to lower binding energies must be due to partial decomposition in the X-ray beam. Differential charging cannot account for this effect because a comparable tailing was not observed in any other signal. Loss of water of hydration and solvating acetic acid leads to a general broadening of all XPS signals except O 1s (as expected), but not to tailing. At 423 K, most of the Pd is reduced to the element, with the expected binding energy of 335.5 eV.[16, 26] The broadening to higher binding energies is evidence that some unreduced Pd remained in the sample. The Pd binding energy is insensitive to the formation of interstitial carbon that is not a carbide. Unfortunately, therefore, we cannot directly deduce the presence of interstitial carbon from XPS. It is highly relevant (Figure 5 right) that the Cd species is still present in its divalent form at 423 K. The complex is separated at that temperature into elemental Pd particles and Cd acetates. A spatial segregation of Pd from the Pd – Cd complex crystals may be deduced from the decrease in the Pd 3d intensity and the sharpening of the peak profile which were observed after heat treatment at 473 K. Metallic Pd therefore appears to be segregated to the surface of the decomposing crystals.

The Cd acetate is decomposed to elemental Cd, as evidenced by the binding energy of 404.4 eV after annealing at 473 K (Figure 5 right). After treatment at 523 and 573 K, Cd was reoxidised, as indicated by XPS. This observation is in agreement with the weight loss estimations. The segregated Pd metal disappeared from the surface, which was covered by carbonaceous species, as indicated by the reversal of the relative intensities of the aliphatic C 1s and Pd 3d signals in the spectra recorded after treatment at 423 and 473 K (see Figures 4 and 5 left). At 573 K, a strong increase in intensity of the 285 eV aliphatic C 1s signal was detected, from which it may be concluded that carbonaceous species are deposited on the surface of the Pd particles. This deposition may occur by exsolution of interstitial carbon in Pd, after which the Pd also



0947-6539/98/0408-1466 $ 17.50+.50/0 *Chem. Eur. J.* **1998**, *4*, No. 8

became oxidised. In the UHV environment of the XPS apparatus, the only source of oxygen available was the remaining acetate ligands, which may have acted as oxidising agents. Consistently, the carboxylic C 1s XPS signal could no longer be detected after this treatment step (Figure 3).

The XPS analysis shows that a mixture of carbon, Pd oxide and Cd oxide is present after pure thermal activation in inert atmosphere. The Pd oxide seems to have been formed from an reduced intermediate Pd species. It may be suggested that, prior to exsolution, interstitial carbon prevented the instantaneous reaction of the freshly reduced Pd particles with oxidising species. As a consequence, it seems appropriate to activate catalysts based upon this complex in a reducing atmosphere of a hydrocarbon. XPS analysis also clearly shows the absence of any Pd–Cd alloy as the ligands are removed from the two constituents at quite different reaction temperatures.

The temperature window of the catalyst activation ends below 520 K at which temperature all catalytic activity should be developed. Generally, a low activation temperature and a high thermal stability of the active metal towards sintering is desirable in order to maintain maximal Pd dispersion. The activation temperature of 425 K for the supported catalyst (vide supra) is lower than indicated in Figure 2, probably because of the dispersion of the precursor, the presence of reductive gases and the modification of the heating programme.

The relevance of the heating programme to the decomposition temperature, which indicates the operation of kinetic influences on the gas–solid-state reactions involved in the ligand abstraction/destruction processes, was studied in a series of TG experiments with variable heating rates (data not shown). The dependence of the temperatures of maximum decomposition rate on the heating rate fitted well to a logarithmic relationship from which we obtained isothermal conversion temperatures for the three main weight loss steps at 342, 438 and 488 K. It is concluded that low heating rates, and eventually a holding interval at about 440 K, would be suitable for minimising the thermal load on the Pd clusters during activation. Between the second and third decomposition steps, a clear plateau was discernible at low heating rates, which confirms the interpretation of the change in the reaction pathway of the acetate decomposition, that has already been deduced from the data of Figure 3.

**The supported Pd–Cd complex**: The red shift in the UV/Vis absorption maximum of the binuclear complex relative to that of Pd acetate (Figure 8A) is in agreement with the in-plane geometry of the Pd–Cd complex determined by X-ray structure analysis. This geometry leads to a destabilisation of the $d_{x^2-y^2}$ orbital relative to that in the out-of-plane distorted Pd complex. The position of the maximum absorption in the UV/Vis spectrum of the impregnated Pd–Cd/$SiO_2$ catalyst is very similar to that of the complex in solution. The shoulder at 400 nm, however, proves that partial decomposition occurs upon interaction with the $SiO_2$ surface. The broken line in Figure 8B is the difference spectrum of supported Pd–Cd acetate minus that of supported Pd acetate. This calculation shows that the binuclear complex is decomposed upon interaction with the $SiO_2$ support, during either impregnation or drying of the catalyst. A quantitative estimate, with the assumption that the absorption coefficents do not change upon interaction with the support, points to 20% decomposition of the Pd–Cd complex.

This decomposition is confirmed by DRIFTS (Figure 9), which produces a completely different spectrum after adsorption on $SiO_2$. Three bands are detected at 1732, 1570sh and 1297 $cm^{-1}$ in the DRIFT spectrum of the adsorbed Pd–Cd complex, which are observed neither in the spectrum of the pure complex nor in that of acetic acid on $SiO_2$. This observation also points to a partial decomposition of the Pd–Cd complex, as already demonstrated by UV/Vis spectroscopy.

The Pd 3d spectra of the pure and the supported precursor compound (Figure 10) also indicate a partial decomposition of the supported Pd–Cd complex, of which the binding energy is about 1 eV lower than that of the unsupported complex. This shift in binding energy (BE) may arise from the exchange of acetate ligands for surface oxygen ions (for Pd $3d_{5/2}$ of PdO, BE = 337.5 eV) or from X-ray-induced decomposition as reported for supported Pd acetate. Exactly such an observation was made for Pd acetate supported on $SiO_2$. In contrast to the unsupported complex, elemental palladium was only detected after thermal decomposition of the supported sample at 573 K in UHV (Figure 11). The much higher decomposition temperature, compared with the unsupported complex, may also point to ligand exchange. It may be concluded that the decomposed, oxidic Pd surface complexes can only be reduced at higher temperatures than the pure Pd–Cd acetate. Consequently, pure palladium acetate adsorbed on $SiO_2$ is reduced to its metallic state after UHV decomposition at the relatively high temperature of 523 K, as shown by XPS. The difference of 150 K between the decomposition temperatures observed for the supported Pd–Cd complex and for the unsupported material is therefore in line with the partial decomposition of the complex upon adsorption and drying, detected by UV/Vis and DRIFTS. It is suggested that this higher stability towards reduction of the Pd species generated from the Pd–Cd precursor has a strong influence on the evolution of the active catalyst material; in particular, particle growth and sintering may be prevented during the activation or the catalytic action. This hypothesis was proved correct by TEM investigations of the used catalysts.

TEM of the used catalyst materials is illustrated in Figure 12. Decomposition of palladium acetate generally led to agglomerated particles, as shown in Figure 12 top. Only a very few small particles were observed. Pd particle sizes obtained from the Pd–Cd precursor varied in the region of 2 nm (Figure 12 bottom), which was somewhat smaller than the smallest particles formed from the binary palladium acetate precursor. Sintering seemed to be prevented in the case of the Pd–Cd precursor because of its higher thermal stability and a particular surface dilution of the Pd species by CdO, which was shown by XPS. Conversely, the higher dispersion of the Pd species obtained from the Pd–Cd complex may support their stability towards reduction, as demonstrated by XPS.

The formation of $CO_2$ started at 473 K over both samples, as Figure 13A shows. The similar light-off temperature, however, does not indicate similar catalytic activity, as proved by the much higher amount of $CO_2$ produced over the Pd–Cd catalyst than over the Pd-containing material. The reduction of the supported $Pd^{II}$ to a metallic phase took place after treatment at 573 K, as XPS measurements showed (see Figure 11). Keeping the temperature of the reactor at 573 K for 30 min resulted in a massive decrease in $CO_2$ evolution over the Pd–Cd catalyst. This reversible catalyst deactivation is most probably connected with the Pd–Cd decomposition at this temperature that has been detected by XPS. Sintering into small Pd particles occurred during the decomposition/activation phase. The catalyst prepared from pure palladium acetate was also reduced to its metallic state, but extensive sintering during activation led to the evolution of large particles, as shown by TEM, and therefore to low catalytic activity. Figure 13C exhibited $CO_2$ formation during a second period of heating to 573 K. The catalyst prepared from Pd–Cd containing small Pd particles again shows catalytic activity above the light-off temperature, whereas the catalyst containing large Pd particles prepared from palladium acetate remained at a low level of catalytic activity.

## Conclusion

Palladium acetate and cadmium acetate in glacial acetic acid form the very stable complex compound $[CdPd(CH_3COO)_4 \cdot CH_3COOH]_2$, which was characterised by TG and by UV/Vis, IR, NMR and XPS spectroscopy. Elucidation of the crystal structure of the binuclear complex has shown a remarkable coordination of palladium which can be described as sixfold with one unsaturated axial position. The metal ions in the complex are in their divalent state, as shown by XPS and $^{113}Cd$ NMR spectroscopy; this excludes the possibility of a preformed metal–metal bond.

The major advantage of this precursor compound for catalyst preparation is the enhancement of the poor solubility of palladium acetate in acetic acid by formation of this Pd–Cd complex. The action of cadmium acetate as an isoionic additive can be excluded, because the solubility of palladium acetate is not significantly changed by addition of other acetates, such as those of Na and K.

The coordination sphere around the Pd atom can be described as a tetragonal bipyramid with one missing axial ligand. For this geometric reason, it is expected that, upon reaction of the complexes with the ligand system of a solid surface (for example, silica with hydroxyl groups), a direct Pd–surface bond may formed with the ternary compound but not with the binary Pd acetate. The formation of the surface bond may be supported electronically by the presence of one other metal (Cd) in the coordination sphere of the Pd centre. The suggested formation of a direct Pd–surface bond (for example, in a ligand-exchange reaction with the participation of a neighbouring hydroxyl group and desorption of a water molecule) may be of great importance during activation of the catalyst, in which the acetate ligands are removed. With the ternary compound the cluster-to-substrate anchor may not be affected during this activation. With the binary Pd acetate, however, it is unavoidable that the cluster-to-substrate bond, which supposedly occurs through acetate ligands, is destroyed during activation. The consequence may be that the resulting ligand-free Pd clusters remain fixed to the surface when they originate from the ternary precursor, but are mobile on the surface and can agglomerate easily when they originate from the binary compound. In addition, the readily soluble ternary precursor will be highly dispersed after the impregnation because the ligand exchange reaction will be complete. Precipitation of unconverted Pd acetate may occur easily and give rise to large Pd particles after activation. Each effect will lead to a different degree of dispersion of the activated Pd on the support and thus affect the ratio of reactive metal surface area exposed per unit surface area of support.

A further advantage of this precursor compound is the small size of the catalytically active Pd particles which are formed during activation. Sintering seems to be avoided by a dilution effect by CdO species. However, we still have no evidence on whether this dilution effect also occurs in a catalyst which is prepared by sequential impregnation of cadmium acetate and palladium acetate.

The formation of a Pd–Cd alloy, proposed to be the active catalyst, must be excluded. Metallic Pd or Pd-containing interstitial carbon is suggested to be the active catalyst. Cadmium plays the important role of a structural promoter. The catalyst formed from the supported binuclear complex is more active in the formation of $CO_2$ from ethylene than that formed from the binary palladium acetate, as IMR-MS measurements have shown. The catalyst activity is referenced to the mass of Pd in the samples, so the different activities observed reflect the different degrees of Pd dispersion. From the improved reactivity of the material derived from the Pd–Cd complex, we conclude that the active surface area is the decisive factor in its behaviour in catalysis.

## Experimental Section

$[Pd(CH_3COO)_2]_3$ (286 mg, 0.425 mmol) and $Cd(CH_3COO)_2 \cdot 2H_2O$ (259.3 mg, 0.973 mmol) were dissolved in glacial acetic acid (4.64 g) at 338 K. The clear orange solution obtained was evaporated, and an orange cystalline solid was isolated which was recrystallised from acetic acid. The supported precursor was prepared by incipient wetness impregnation by adding 0.5 g of the acid solution to $SiO_2$ (2.13 g) with vigorous stirring at 300 K. The sample was dried in vacuum at 300 K for 2 h.

TG was performed on an FSC 5200 thermogravimetric balance (Seico). The measurements were taken under an argon atmosphere (gas flow 100 mL min$^{-1}$) with a sample weight of about 10 mg.

UV/Vis spectra were obtained on a Perkin-Elmer spectrophotometer, model 555. For solutions, cuvettes with an optical pathlength of 1 cm were used. The spectra were measured against glacial acetic acid (Fluka) as reference. To investigate solids, a diffuse reflectance attachment was used with pure $SiO_2$ as reference.

NMR spectra were measured on a 400 MHz instrument (JEOL). The pure solids were dissolved in $D_2O$. $^{13}C$ NMR investigations were performed at 100.40 MHz, using TMS as external standard. $^{113}Cd$ resonances were observed at 88.55 MHz with cadmium perchlorate as external standard.

The DRIFTS measurements were conducted under a helium atmosphere (gas flow 50 mL min$^{-1}$) on a Bruker IFS 66 spectrometer with a DRIFTS unit (Graseby/Specac P/N 19900) and an in-situ cell (Graseby/Specac P/N 19930).



0947-6539/98/0408-1468 $ 17.50+.50/0 *Chem. Eur. J.* **1998**, *4*, No. 8

XPS investigations were performed on an LHS 12 MCD (Leybold) instrument with a magnesium anode (power 14 mA = 168 W, pass energy 108 eV). The samples were suspended in hexane and deposited on a gold foil. Spectra were recorded at room temperature after the samples had been heated for 30 min at given temperatures and at nitrogen pressure 1 bar. The resolution of the equipment was determined from the Ag $3d_{5/2}$ signal to be 1.2 eV. The binding energies of the sample are referred to the Si 2p peak at 103.6 eV for $SiO_2$ and to the C 1s peak at 285.0 eV for $CH_3$ groups as standards.

IMR-MS measurements were executed on an Atomika 1500 spectrometer. The ion–molecule reactions occurred in an octupole reaction chamber, with xenon and krypton as primary ions. A quadrupole mass detector was used in combination with suitable ion-extraction optics. Further details have been reported in the literature.[27]

TEM investigations were performed on a Philips CM 200 FEG microscope equipped with energy dispersive X-rays (EDX). The total magnification for Figure 11 was $\times 405\,000$ at 200 k eV. The supporting grids gave rise to the intense Cu and weak Mg EDX signals.

For the ethylene oxidation, $C_2H_4$ (99.95 % grade; Linde) was used. $SiO_2$ (600 mg; BET specific surface area 159 $m^2 g^{-1}$) was impregnated with a solution (0.5 g) of $[Pd(CH_3COO)_2]_3$ (291.5 mg in 4.6 g glacial acetic acid). A portion (36.4 mg) of the dried sample was placed in the centre of a quartz tube reactor (diameter 8 mm), which was filled with quartz wool (hourly space velocity (hsv) = 51.5 $h^{-1}$; BET surface areas 133 and 130 $m^2 g^{-1}$ for supported Pd acetate and Pd–Cd acetate, respectively). During activation, the reactor was flushed with nitrogen (200 mL $min^{-1}$), and the temperature was ramped with a heating rate of 0.5 K $min^{-1}$. The temperature was kept constant at 428 K for 30 min. At this temperature (after a time on stream, $t$, of 250 min), $C_2H_4$ was added to the atmosphere at a flow rate of 25 mL $min^{-1}$, then oxygen was added at a flow rate of 4 mL $min^{-1}$ at 428 K and $t = 260$ min. At $t = 280$ min, the reactor was heated to 573 K at a rate of 0.5 K $min^{-1}$. The temperature of the reactor was kept constant at 573 K for 30 min, reduced to 373 K (5 K $min^{-1}$), then kept constant for 10 min before the reactor was reheated to 573 K.

The Pd–Cd/$SiO_2$ sample was treated as described above for the Pd/$SiO_2$ catalyst. A portion (55 mg) of the Pd–Cd/$SiO_2$ sample was used for the experiment, which was conducted under similar conditions (hsv = 34.1 $h^{-1}$).

**$[CdPd(CH_3COO)_4 \cdot CH_3COOH]_2$**: UV/Vis (acetic acid): $\delta_{max} = 343$ nm; UV/Vis (on $SiO_2$): $\delta_{max} = 340$ nm; $^{13}C$ NMR: $\delta = 31.030$, 22.295 ($CH_3$), 216.210, 179.692 ($COO$); $^{113}Cd$ NMR: $\delta = 17.66$.

**Acknowledgments:** The authors are indebted to D. Herein, Prof. R. J. Behm and his co-workers for useful discussions, and to N. Pfänder for the TEM investigations. This work was supported financially by the Fonds der Chemischen Industrie.

Received: July 29, 1997 [F785]

[1] K. Weissermel, H.-J. Arpe, *Industrielle Organische Chemie. Bedeutende Vor- und Zwischen-produkte*, 4th ed., VCH, Weinheim, **1994**, pp. 247–252.
[2] T. Tisue, W. J. Downs, *J. Chem. Soc. Chem. Commun*. **1969**, 410.
[3] A. S. Abu-Sarrah, B. Rieger, *Angew. Chem*. **1996**, *108*, 2627; *Angew. Chem. Int. Ed. Engl.* **1996**, *35*, 2475.
[4] J. Louie, J. F. Hartwig, *Angew. Chem*. **1996**, *108*, 2531; *Angew. Chem. Int. Ed. Engl.* **1996**, *35*, 2359.
[5] a) W. Schwerdtel, *Chem.-Ing.-Techn*. **1968**, *40*, 781–784; b) Review: R. F. Heck, *Org. React*. **1982**, *27*, 345.
[6] L. Eberson, L. Gomez-Gonzalez, *Acta Chim. Scand*. **1973**, *27*, 1162, 1249.
[7] P. Y. Johnson, J. Q. Wen, *J. Org. Chem*. **1981**, 2767.
[8] A. C. Skapski, M . L. Smart, *J. Chem. Soc. Chem. Commun.* **1970**, 658.
[9] N. N. Lyalina, S. V. Dargina, A. N. Sobolev, T. M. Buslaeva, I. P. Romm, *Koord. Khim*. **1993**, *367*, 57.
[10] F. A. Cotton, G. Wilkinson, *Advanced Inorganic Chemistry*, John Wiley, New York, **1980**.
[11] W. Harrison, J. Trotter, *J. Chem. Soc. Dalton, Trans.* **1972**, 956.
[12] J. N. van Niekerk, F. R. L. Schoening, *Acta Crystallogr*. **1953**, *6*, 227.
[13] G. A. Somorjai, *Introduction to Surface Chemistry and Catalysis*, Wiley Interscience, New York, **1994.**
[14] M. Neumann, R. Schlögl, *Langmuir,* submitted.
[15] V. I. Nefedov, Y. V. Salyn, I. I. Moiseev, A. P. Sadovskii, A. S. Berenbljum, A. G. Knizhnik, S. L. Mund, *Inorg. Chim. Acta* **1979**, *35*, L343.
[16] C. D. Wagner, W. M. Riggs, L. E. Davis, J. F. Moulder, G. E. Muilenberg, *Handbook of X-Ray Photoelectron Spectroscopy*, Perkin-Elmer, **1979**.
[17] T. A. Stephenson, S. M. Morehouse, A. R. Powell, J. P. Heffer, G. Wilkinson, *J. Chem. Soc*. **1965**, 3632.
[18] L. H. Jones, E. McLaren, *J. Chem. Phys.* **1954**, 22, 1796.
[19] K. J. Wilmshurst, *J. Chem. Phys.* **1955**, 23, 2463.
[20] K. Ito, H. J. Bernstein, *Can. J. Chem.* **1956**, *34*, 170.
[21] K. Nakamoto, *Infrared Spectra of Inorganic and Coordination Compounds*, John Wiley, New York, **1963**, p. 197ff.
[22] G. B. Deacon, R. J. Phillips, *Coord. Chem. Rev.* **1980**, *33*, 227.
[23] R. W. Brandon, D. V. Claridge, *Chem. Commun.* **1968**, 677.
[24] H. Nowotny, A. Stempfl, E. Bauer, H. Bittner, *Monatsh. Chem*. **1950**, *81*, 887, 1164; *ibid*., **1951**, *82*, 949.
[25] M. Hansen, *Constitution of Binary Alloys*, McGraw-Hill, New York, **1958**.
[26] V. I. Nefedov, Y. V. Salyn, I. I. Moiseev, A. P. Sadovskii, A. S. Berenbljum, A. G. Knizhnik, S. L. Mund, *Inorg. Chim. Acta* **1979**, *35*, L343.
[27] H. Schubert, H. Hertle, T. Rühle, H. Werner, R. Schlögl, *IMR-MS. Eine Methode zur Analyse komplexe Emmissionsgase*, VDI Paper No. 1257, **1996**.
[28] Crystallographic data (excluding structure factors) for the structures reported in this paper have been deposited with the Cambridge Crystallographic Data Center as supplementary publication no. CCDC-100540. Copies of the data can be obtained free of charge on application to CCDC, 12 Union Road, Cambridge CB2 1EZ, UK (fax: (+44) 1223-336-033; e-mail: deposit@ccdc.cam.ac.uk).